


Experimental and numerical investigation of the uncut chip thickness reduction in Ti6Al4V orthogonal cutting

F. Ducobu  · E. Rivière-Lorphèvre · E. Filippi

Received: 25 February 2016 / Accepted: 14 July 2016 / Published online: 19 July 2016
© Springer Science+Business Media Dordrecht 2016

Abstract The downsizing of traditional cutting (“macro-cutting”) to micro-cutting introduces changes in the cutting process. The uncut chip thickness decreases and the cutting edge radius of the tool cannot be neglected anymore. The minimum chip thickness phenomenon takes importance, as well as ploughing. The size effect appears and the influence of the microstructure grows. Determining the value of the uncut chip thickness is a major concern to produce high quality parts. This paper focuses on the determination of that value experimentally with a setup providing strictly orthogonal cutting configuration and a one-time machining of the surface, as well as numerically with a finite element model by only changing the value of the uncut chip thickness. Specificities of micro-cutting are highlighted experimentally and numerically. The cutting refusal is observed in both cases and the minimum chip thickness is estimated (at minimum 25 % of the cutting edge radius) with a good correlation.

Keywords Experiments · Finite element · Micro-cutting · Minimum chip thickness · Orthogonal cutting · Titanium alloy Ti6Al4V

1 Introduction

Parts and features ranging from several mm to several μm are more and more asked in the current context of miniaturization. Micro-manufacturing technologies by removal of material can be used to produce that type of parts; micro-milling is one of them. Similarly to traditional (“macro-”) milling, complex tridimensional micro-forms including sharp edges and a good surface finished can be obtained quickly [1, 2] and without the need of expensive tooling. Micro-milling is based on macro-milling but the micro-cutting process is not a direct down-scaling of macro-cutting as some changes occur in the cutting phenomenon. In macro-cutting, the uncut chip thickness is generally larger than the cutting edge radius of the tool. Consequently, the chip formation models consider that the tool cuts the material and generates chips. This is not valid anymore in micro-cutting [1, 3, 4] especially because the tool dimensions decrease. The cutting edge radius is not reduced proportionally to the other dimensions: its reduction is limited due to the manufacturing process limitations (it is currently of the order of 1–4 μm in micro-milling [5]) and the tool cannot be considered as sharp anymore. This leads the uncut chip thickness to be often smaller than the cutting edge radius.

Micro-cutting introduces several differences by comparison to macro-cutting. One of the main concern is the transition from cutting to ploughing when the

F. Ducobu (✉) · E. Rivière-Lorphèvre · E. Filippi
Machine Design and Production Engineering Lab, Faculty
of Engineering (FPMs), University of Mons (UMONS),
20 Place du Parc, 7000 Mons, Belgium
e-mail: Francois.Ducobu@umons.ac.be

uncut chip thickness decreases. Knowing this transition value (i.e. the “minimum chip thickness”) is therefore of great interest for the nature of the process and the quality of the produced part. Up to now, few finite element models dealing with micro-cutting are found in the literature. None is available to highlight the cutting refusal and provide a quantitative estimation of the minimum chip thickness with an experimental validation in orthogonal cutting. This research focuses on that transition and on the determination of the minimum chip thickness value in the simplified configuration of orthogonal cutting, studied both experimentally and numerically. To do that, a dedicated experimental setup is used. It ensures that the cutting is strictly orthogonal and that the surface is machined only once. This allows to compare directly the results with the finite element model developed in the same cutting conditions. The model does not change between macro- and micro-cutting conditions. The differences in the chip formation are due to the decrease of the uncut chip thickness. No other modification of the model is required to handle micro-cutting conditions.

This paper begins with a review of the literature and the differences introduced by the transition from macro- to micro-cutting. The motivations of this work are given before the presentation of the finite element model and the experimental setup in strictly orthogonal cutting conditions. The next section gathers the results comparing the experiments and the numerical model on the chip formation and morphology, the cutting forces, the specific cutting energy and the elastic spring-back of the workpiece. It is followed by a summary of the findings on the evolution of the cut from macro- to micro-cutting conditions, before the conclusions.

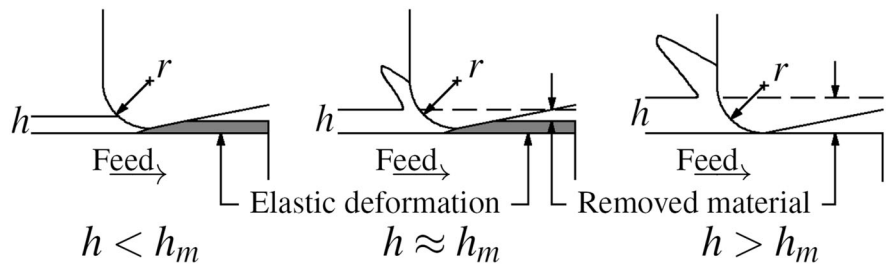
2 Literature review

The significant importance of the “minimum chip thickness” phenomenon is the main difference in the chip formation between the macro-cutting and micro-cutting processes [1]. It is defined as the smallest uncut chip thickness value allowing to form a chip [1]. According to Filiz et al. [6] and Chae et al. [1], it is often evaluated between 5 and 38 % of the tool edge radius, depending on the machined material. A more recent work from de Oliveira et al. [7] concludes that

the minimum chip thickness value goes from 1/4 to 1/3 of the cutting edge radius for any machined material, tool geometry and method to estimate it. Figure 1 shows the three configurations that can occur in micro-cutting. When the uncut chip thickness, h , is below the minimum chip thickness, h_m , ($h < h_m$) the workpiece is elastically and plastically deformed and no chip is formed. Deformations and friction forces dominate the process. When the uncut chip thickness is close to the minimum chip thickness ($h \approx h_m$), high deformations still occur on the machined surface but a chip is formed. The elastic spring-back of the workpiece after the tool tip passage is large and the thickness of the removed material is smaller than the uncut chip thickness. The roughness of the machined surface is high and there are several burrs, as the material is more torn than deformed and sheared. When the uncut chip thickness is larger than the minimum chip thickness ($h > h_m$), the deformations of the workpiece are negligible and the thickness of removed material is very close to the uncut chip thickness; this configuration is the same as in macro-cutting.

A rising of the slipping forces and the ploughing of the machined surface due to the minimum chip thickness is highlighted by Bissaco et al. [8]. This contributes to the increase of the cutting forces, the burrs formation and the surface roughness. Vogler et al. [9–11] investigated experimentally and numerically the influence of the minimum chip thickness on the cutting forces in micro-milling. They observed that the teeth of the tool can only deform the material without forming any chip when the feed is too low. A chip is formed later, when the accumulated material becomes larger than the minimum chip thickness. This was observed in micro-milling of Ti6Al4V by Ducobu et al. [12]: a chip is formed after several tool rotations when the feed per tooth is smaller than the minimum chip thickness. In the same study, they showed that, contrary to macro-milling, the stability of the operation can be feed dependent. Jun et al. [13] measured, for ferrite, that when the uncut chip thickness decreases, the thrust force becomes larger than the cutting force. Liu et al. [14] presented an analytical model to predict the minimum chip thickness value from the thermomechanical properties of the machined material. The minimum chip thickness depends on the material; Son et al. [15] therefore considered the influence of friction between the tool and the workpiece. They expressed analytically the

Fig. 1 Schematic representation of the minimum chip thickness in orthogonal cutting (r : edge radius of the tool, h : uncut chip thickness, h_m : minimum chip thickness), inspired from [1]



value of the minimum chip thickness in function of the tool edge radius and the friction angle between the tool and the chip. They observed that the roughness of the machined surface is the lowest at the minimum chip thickness, while de Oliveira et al. [7] found that it occurs at an uncut chip thickness value between the minimum chip thickness and the cutting edge radius value. In another study, Son et al. [16] studied the influence of vibration assisted cutting on the minimum chip thickness. They noted that the vibrations increase the friction coefficient between the tool and the workpiece, which leads to the reduction of the minimum chip thickness.

In micro-cutting, the tool can no longer be assumed as sharp and it does not completely cut the material to generate chips. This is due to the chip thickness smaller than the cutting edge radius, which leads to a negative effective rake angle [3]. A highly negative rake angle causes ploughing of the machined surface and thus a poor surface roughness and a large elastic spring-back [17]. The spring-back fraction occurring under the flank face generates friction that rises the specific cutting energy [17]. Kim and Kim [18] developed an analytical model taking the cutting edge radius and the elastic spring-back into account, inducing an increase of friction along the flank face.

The “size effect” phenomenon was observed by Filiz et al. [6] at small uncut chip thickness. It consists of a nonlinear increase of the specific cutting energy when the uncut chip thickness decreases. This phenomenon would be due to the large deformation of the material caused by the negative effective rake angle [6] (Liu et al. [19] noted that this is the main contribution to the size effect), the pressure on the flank face due to the elastic spring-back [6], the rise of the friction forces on the flank face and the contact length with the tool [6, 19], the dislocation density [6] and the widening of the primary shear zone due to the edge radius, which requires a larger energy dissipation

[19]. Liu et al. [19] recommended to take into account the strain gradients in the machined material in micro-cutting. An increase in the cutting force and vibrations was noticed by Ducobu et al. [12] when the size effect and the minimum chip thickness were taken into account. The vibrations magnitude was significant as it could be larger than the required tolerance of the part.

The macro-cutting assumption of a material that is homogeneous and isotropic is no longer valid in micro-cutting. This is a consequence of the reduction of the different dimensions to consider in the process (uncut chip thickness, tool edge radius, feature to be machined) that become equal or smaller than the grain size [1, 3]. The granular structure of the machined material should be taken into account [1, 3]. The lack of homogeneity of the material (hardness mainly) leads to the cutting forces variations, inducing vibrations [1, 3, 11]. Contrary to a macro-cutting operation, the cutting conditions or the machine design modification is of no help to get rid of them. This also implies that the averaged macro-cutting coefficients are no longer valid in micro-cutting.

There are not many finite element modeling dealing with micro-cutting in the literature. Woon et al. [20] developed an ALE orthogonal cutting model of AISI 4340 steel in 2D. The material is considered as homogeneous. The tool is rigid and its edge radius influence on chip formation is studied. The conclusions were that the geometry and the value of the edge radius should be taken into account in future works as they play a key role in the chip formation. Liu et al. [19, 21] showed, with a 2D finite element model, that the strain gradient strengthening is the main contributor to the size effect in micro-cutting for a material with a small strain rate hardening exponent such as the aluminium alloy Al5083-H116. Ohbuchi and Obikawa [22] developed an orthogonal cutting finite element model with a highly negative rake angle. They observed that a small fraction of the chip, triangular

and called “stagnant chip”, is in front of the tool and slides with difficulty along the rake face. Its size grows for a more negative rake angle and is proportional to the uncut chip thickness. It acts as a built-up edge, except that its shape and its size do not change during the cut and that it does not come off the workpiece. They observed that there are a cutting speed and an uncut chip thickness, depending on the rake angle, for which this chip does not form. A 2D orthogonal cutting finite element model of AISI 1045 steel with a sharp tool was developed by Simoneau et al. [23]. The material was heterogeneous to take the granular structure of the material into account in the chip formation. The “quasi-shear extrusion chip” was observed. It consists of the extrusion of the softest material (ferrite) between the grains of the hardest material (pearlite). That type of chip formation is only possible when the material is considered as heterogeneous, which was recommended by the authors for AISI 1045 micro-cutting. For Ti6Al4V, Zhang et al. [24], presented a finite element macro-cutting model with a material microstructure-level model based on the crystal plasticity theory. The grains were explicitly taken into account and the main source of heterogeneity came from the grains orientation angles and the slip system strength anisotropy. The Ti6Al4V considered is composed of only a primary α phase. They showed the influence of the microstructure on the chip formation and the surface integrity.

3 Motivations of the study

The literature review showed no work strictly focused on the comparison and validation of finite element and experimental results on the evolution of the chip formation depending on the uncut chip thickness value, with an estimation of the minimum chip thickness value. This paper proposes to fill this gap by providing a study of the chip formation and morphology, cutting forces and specific cutting energy evolutions when the uncut chip decreases. It will be performed both numerically and experimentally in the simplified frame of orthogonal cutting. Particular care will moreover be taken to ensure that the experiments are conducted in strictly orthogonal cutting (cf. Sect. 5) to allow for a rigorous comparison with the modeling. This numerical model (cf. Sect. 4) has already been validated in macro-cutting conditions

[25, 26] and was developed with the constraint to respect the physical phenomena and not influence the chip formation (with a predefined chip separation line, for example [27]) [25]. The model will have to be able to deal with the absence of chip formation and/or the formation of a chip with a chip thickness smaller than the specified value. This is why the path along which the chip should/could separate of the workpiece (typically called “sacrificial layer” [28] or “separation line” [29]) will not be defined, contrary to models of Mabrouki et al. [27], Zhang et al. [30] or Ducobu et al. [31] for examples. To compare with the experiments, the chip morphology should be close to the experiments. This will be better achieved with a Lagrangian formalism than an ALE formalism [25]. The formalism adopted for this work will therefore be Lagrangian. The contribution of this paper consists in the numerical and experimental estimation of the minimum chip thickness value, as well as in highlighting the specificities of micro-cutting, the cutting refusal and the changes in the chip formation mechanisms when the uncut chip thickness decreases, both numerically and experimentally.

4 Finite element model

A major constraint on the model is that it has to deal with several uncut chip thicknesses leading to different chip formation mechanisms (ranging from segmented, or saw-toothed, chip to the cutting refusal) without any other change than the uncut chip thickness value. This is a fundamental feature of the model as the uncut chip thickness ranges from macro- to micro-values and the cutting refusal has to be handled. It was not optimized to model a particular cutting condition but to respect the mechanisms of chip formation. The model has previously been experimentally validated in macro-cutting conditions [26]. In this study, cutting conditions are expanded from macro- to micro-cutting.

The finite element model was developed with the commercial software ABAQUS/Explicit v6.11 in order to study numerically the Ti6Al4V chip formation [25, 26]. It is a 2D plane strain orthogonal cutting model taking into account the area close to the cutting edge of the tool. The basic idea is to be in “geometrical” micro-cutting conditions (ratio between the

Table 1 Material properties and cutting conditions of the numerical model [26, 33, 36–38]

TANH model	A (MPa)	1936
	B (MPa)	380
	C	0.02
	m	0.577
	n	0.421
	T_{room} (K)	298
	T_{melt} (K)	1878
	a	1.6
	b	0.4
	c	6
d	1	
Inelastic heat fraction	Ti6Al4V	0.9
Density, ρ (kg/m ³)	Ti6Al4V	4430
	Carbide	15,000
Young’s modulus, E (GPa)	Ti6Al4V	113.8
	Carbide	800
Expansion, α (K ⁻¹)	Ti6Al4V	8.6×10^{-6}
	Carbide	4.7×10^{-6}
Conductivity, k (W/mK)	Ti6Al4V	7.3
	Carbide	46
Specific heat, c_p	Ti6Al4V	580
	Carbide	203
Friction coefficient		0.05
Friction energy to heat (%)		100
Heat partition to part (%)		25
Cutting speed (m/min)		30
Uncut chip thickness (μm)		280, 100, 40, 20,
		10, 5, 2.5, 1
	Rake angle ($^\circ$)	15
	Clearance angle ($^\circ$)	2
Cutting edge radius (μm)		10

uncut chip thickness, h , and the cutting edge radius, r , smaller than 1: $h/r < 1$).

The tool geometry and the cutting conditions are the same as for the experimental study: a rake angle of 15°, a clearance angle of 2°, a cutting edge radius of 10 μm , a cutting speed of 30 m/min and eight uncut chip thicknesses values (Table 1). The workpiece is modeled as a rectangular box and is fixed in space (Fig. 2). To limit the CPU computing time, its dimensions are reduced when the uncut chip thickness decreases. The length of the elements in the upper part of the workpiece depends on the uncut chip thickness value (5 μm for $h = 280$ and 100 μm , 1 μm for $h = 40$, 20 and 10 μm , 0.25 μm for $h = 5$, 2.5 and 1 μm). This

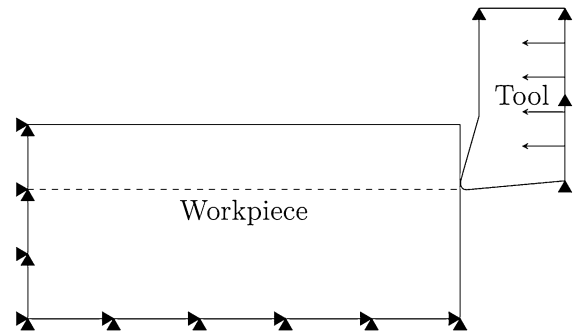


Fig. 2 Boundary conditions and initial geometry

length was chosen to ensure that the uncut chip thickness is made of at least 8 elements (except for 1 μm : 4 elements). Adaptive mass scaling is introduced in the model with a minimum time increment value equal to 10 % of the initial time increment value, in accordance with [32].

The machined material is considered as homogeneous and it is described by the TANH model introduced by Calamaz et al. [33]. This is assumed to be sufficient to expand to micro-cutting conditions a model validated in macro-cutting conditions. Empirical constitutive models are moreover still widely used when modeling micro-cutting [20, 23]. The TANH model consists of an upgraded Johnson–Cook model [34] to take strain softening into account. In the recent literature, an increasing number of authors [25, 33, 35] recommends to take the strain softening into account in finite element modeling, regardless of the finite element software, to form realistic Ti6Al4V chips.

The TANH equation is expressed as follows [33]:

$$\sigma = \left[A + B \varepsilon^n \left(\frac{1}{\exp(\varepsilon^a)} \right) \right] \left[1 + C \ln \frac{\dot{\varepsilon}}{\dot{\varepsilon}_0} \right] \left[1 - \left(\frac{T - T_{room}}{T_{melt} - T_{room}} \right)^m \right] \left[D + (1 - D) \tanh \left(\frac{1}{(\varepsilon + S)^c} \right) \right] \quad (1)$$

with

$$D = 1 - \left(\frac{T}{T_{melt}} \right)^d \text{ and}$$

A , B , C , m and n are material properties having the same meaning as for Johnson–Cook model, while a , b , c and d are the new constants introduced by the

TANH model, T_{melt} is the melting temperature, T_{room} is the room temperature and $\dot{\epsilon}_0$ is the reference strain rate. The value of the A parameter has been adapted from the original article of Calamaz et al. [33] to better describe the metallurgical state of the machined Ti6Al4V of this study [26]. Parameters values are given in Table 1.

The tool material is tungsten carbide and it is described by a linear elastic model. The materials properties of Ti6Al4V and tungsten carbide adopted in the numerical model can be found in Table 1.

Coulomb's friction, with a low coefficient value (0.05) [25], is used to model friction at the tool–chip interface and all the friction energy is converted into heat, which is usually assumed [39]. Only conduction is considered and all the parts faces are adiabatic. The transformation of the deformation to heat is assumed to occur with an efficiency of 90 % [36]. Explicit Lagrangian formulation is adopted and a chip separation criterion must therefore be introduced in the model. It consists of an “eroding” elements method with crack propagation in the workpiece using the temperature dependent tensile failure of Ti6Al4V, as previously presented in [26].

5 Experimental orthogonal cutting setup

The aim of these experiments is to highlight the cutting refusal and the evolution of the chip formation mechanisms with the h/r ratio. Two classical orthogonal cutting configurations are found in the literature [40], both in turning: Altintas [41] performs face turning of the end of a tube with a large diameter and a small thickness (the width of the tool is larger than the thickness of the tube), while Mahnama and Movahhedy [42] carry out plunge turning of large diameter radial grooves having a width smaller than that of the tool. When the sample is cylindrical, its radius influences the cutting due to the curvature of the surface to machine. This radius may disturb the analysis of the results when the uncut chip thickness decreases. It cannot be neglected anymore for very small uncut chip thicknesses, as these considered in this study (or the radius of the sample should increase dramatically), and the process moves away from orthogonal cutting conditions. Moreover, to highlight the absence of chip formation, the cutting tool cannot machine the same surface more than once. The best

configuration would be to use a planning machine, but this equipment is less standard in research labs than a milling machine, moreover with high cutting speeds. Another configuration has therefore been proposed in Ducobu et al. [40] on a milling machine with the constraints to machine the surface only once and to provide strictly orthogonal cutting conditions.

The adopted setup [40] uses a five-axis high speed milling machine Deckel-Maho DMU-80T (positioning accuracy of 1 μm) as a planning machine to remove a layer of material in dry cutting conditions. The thickness of that layer is the uncut chip thickness, constant during a test, and its value can be defined by the user. The positioning accuracy, 1 μm , is equal to the smallest uncut chip thickness of the study. The uncertainty on the actual experimental uncut chip thickness value will grow when h decreases to become equal to it for 1 μm . Results at small h values should therefore be exploited carefully. It is considered that the uncut chip thickness in the experiments is equal to the theoretical value for the comparison with the modeling. The positioning accuracy may however explain, at least partially, some of the differences.

In this configuration (Fig. 3), the cutting movement is an horizontal displacement generated by the sample (inserted into the spindle) with respect to the stationary tool (fixed on the machine table), ensuring that the cutting is really orthogonal. The sample [40] is a cylinder with three parallel tenons of 1 mm wide on its top surface. The width of the tenons is set to 1 mm to minimize the efforts in the spindle bearings and to give the forces value per mm width as in the numerical model.

The cutting speed is set to the maximum feed rate of the machine, 30 m/min. This value is in the range recommended by the tool manufacturer SECO for the standard version of the tool (27–39 m/min) [43]. The tool is placed on the machine table through an interface part fixed on the force sensor. This tool is custom made by SECO to provide a rake angle of 15°, a clearance angle of 2° and a cutting edge radius of 10 μm , as in the numerical model. Eight values of the uncut chip thickness h are adopted, while the cutting speed is kept constant. The cutting conditions of the experimental tests are summarized in Table 2. The Ti6Al4V alloy used for the experiments is annealed (at 750 °C during an hour followed by air cooling) Ti6Al4V grade 5 (AMS 4928). Its main properties

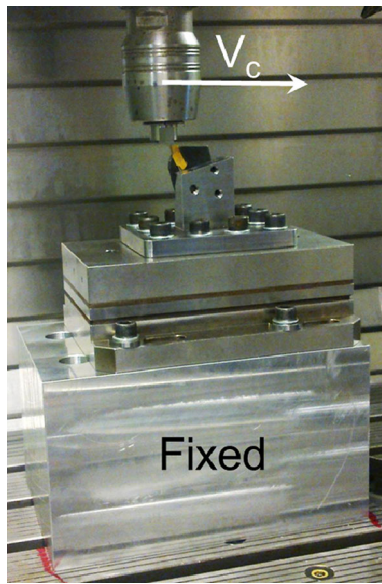


Fig. 3 Orthogonal cutting configuration on the milling machine [40]

Table 2 Cutting conditions

Cutting speed (m/min)	30
Uncut chip thickness (μm)	280, 100, 40, 20, 10, 5, 2.5, 1
Width of cut (mm)	1
Length of cut (mm)	10
Rake angle ($^\circ$)	15
Clearance angle ($^\circ$)	2
Cutting edge radius (μm)	10

and detailed composition according to AMS 4928 standard are available in reference [38].

The cutting forces are measured in the three directions with a Kistler 9257B dynamometer. The rest of the acquisition chain is composed of the multichannel charge amplifier Kistler 5070A, the data acquisition system (DAQ) Kistler 5697A2 and the DynoWare software. Chip formation is observed through a high frequency camera Photron FASTCAM SA3 at an acquisition frequency of 30,000 frames per second with a resolution of 128 pixels \times 128 pixels. After the cut, the chips are collected to be observed through a Keyence VHX-2000 digital microscope. These measurements and observations will allow to compare the chip formation, its morphology, the cutting forces and the specific cutting energy with the numerical model.

6 Results

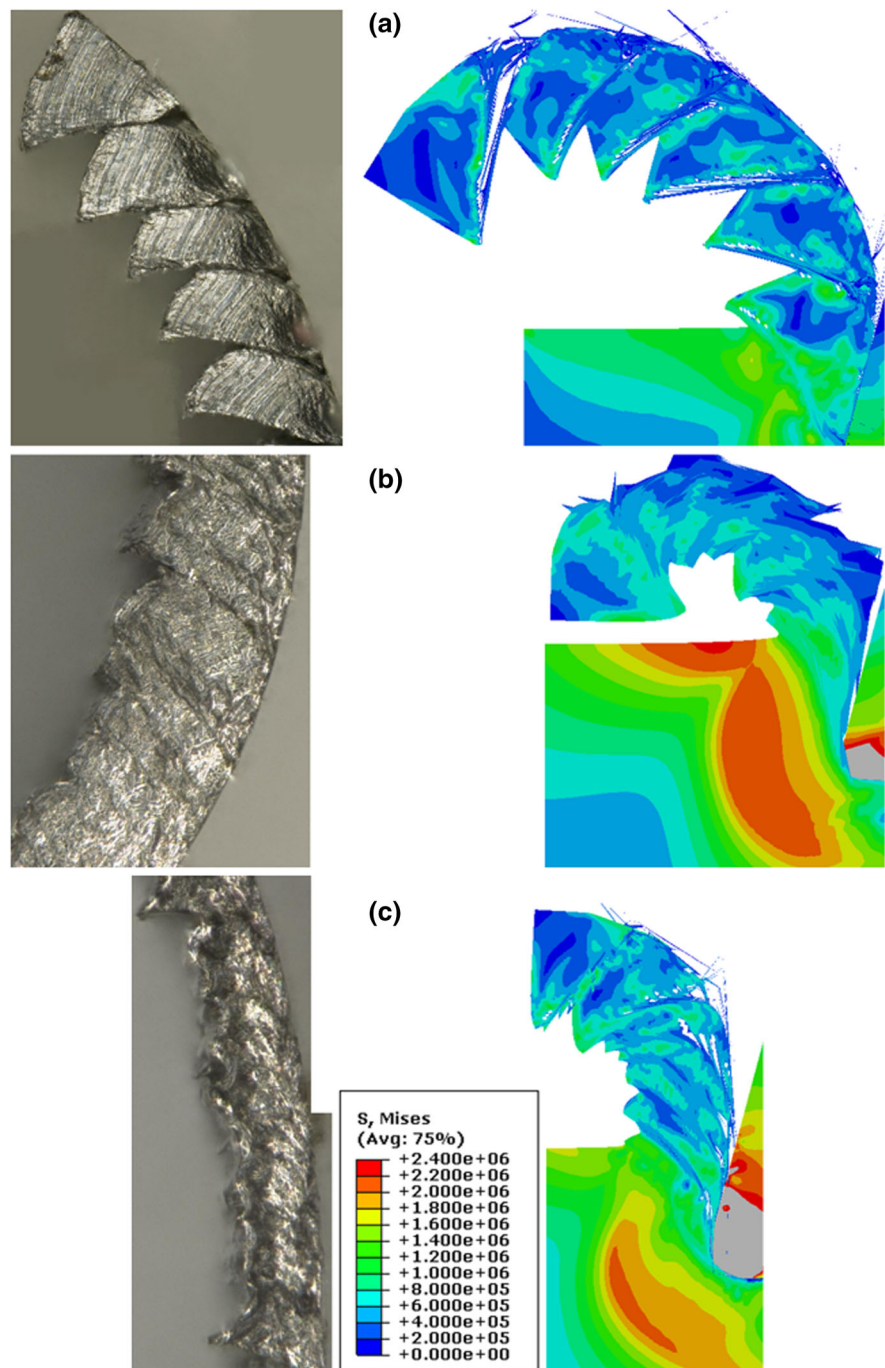
6.1 Chip morphology and formation

Figures 4 and 5 show experimental and numerical chips and machined material deformation for the eight h/r ratios. Experimentally, for $h = 1, 2.5$ and $5 \mu\text{m}$, when a chip was formed, it was too small and fragile to be collected. Moreover, when it was possible to see them, they disintegrated as soon as they were touched. A chip is undoubtedly formed when h/r is larger than 0.5. The chip morphology goes from segmented to no chip including quasi-continuous chip. In Fig. 4a, both chips are segmented and their geometries are close (a quantitative comparison for uncut chip thicknesses larger than $40 \mu\text{m}$ is performed by Ducobu et al. [26]). At $100 \mu\text{m}$ (Fig. 4b), both chips are quasi-continuous, as well as at $40 \mu\text{m}$ (Fig. 4c) although small segments can be seen in this case. For these 3 uncut chip thicknesses, the model gives results close to the experiments. The primary shear zone is easily seen in the modeling and the stresses decrease inside it when a segment is forming, as expected.

Numerical chips from 20 to $5 \mu\text{m}$ (Fig. 5a–c) have irregular segments and their depth vary. The experimental chips for 20 and $10 \mu\text{m}$ are globally quite close to the numerical ones. However, for $10 \mu\text{m}$, the numerical segments differ from the experiments as they are more spaced and less deep. In the modeling, the primary shear zone is wider at this uncut chip thickness.

For the three smallest uncut chip thicknesses (Fig. 5c–e), no experimental chip is available. However, high frequency pictures allow to have information about the chip formation mechanism in the experiments. Some of them are shown in Fig. 6 for two uncut chip thickness values and consist of a projection of the phenomena in the cutting plane. If a lateral bending of the chip occurs out of the cutting plane during its formation, it will not be captured by these pictures. As they aim at getting information on the formation of a chip, the projection in the cutting plane does not alter these observations. A change in the chip formation mechanism is clearly observed when the uncut chip thickness decreases (Fig. 6). Indeed, at $h = 1 \mu\text{m}$, the chip is not formed immediately after the beginning of the cut. The tool moves without producing any chip and the surface of the workpiece is only deformed, as shown in Fig. 6a after

Fig. 4 Numerical [Von Mises stresses contours (e^3 Pa)] and experimental chips **a** $h = 280 \mu\text{m}$, **b** $h = 100 \mu\text{m}$ and **c** $h = 40 \mu\text{m}$



0.6 ms of cut. The deformed material accumulates in front of the tool and this amount grows when the cutting length increases. Once its thickness reaches a breaking value, i.e. the minimum chip thickness, it is torn of the workpiece (Fig. 6b) and the same process

starts again. The cutting refusal is therefore observed and the “chip” is not formed anymore with the classical mechanism of macro-cutting. The distance traveled by the tool before forming a chip decreases when the uncut chip thickness increases and it is close

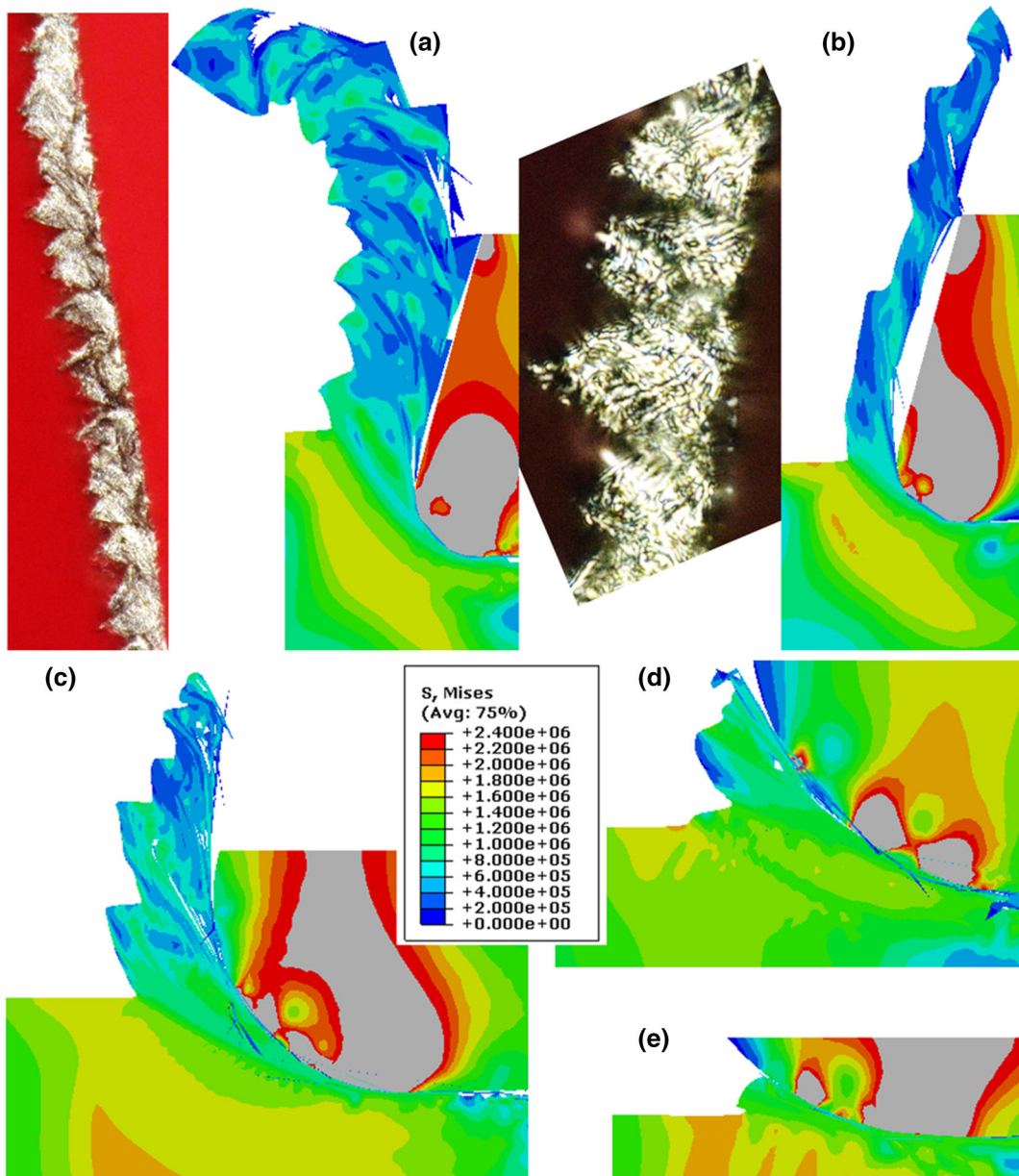


Fig. 5 Numerical [Von Mises stresses contours (e^3 Pa)] and experimental chips **a** $h = 20 \mu\text{m}$, **b** $h = 10 \mu\text{m}$, **c** $h = 5 \mu\text{m}$, **d** $h = 2.5 \mu\text{m}$ and **e** $h = 1 \mu\text{m}$

to zero when $h = 10 \mu\text{m}$. That difference in the chip formation process is clearly seen in Fig. 6c: a chip of a significant length is already formed after 0.6 ms although there is no chip at the same time when the uncut chip thickness is $1 \mu\text{m}$ (Fig. 6a). It should be noted that the side flow of the chip that may occur experimentally is not taken into account in the modeling because the model is in 2D plane strain.

This lateral expansion takes importance when the uncut chip thickness decreases. It leads to a thicker numerical chip that may promote the formation of a chip. However, this difference should not dramatically influence the results as the minimum chip thickness is more a range of values than a single one.

Numerically, Fig. 5d shows that a small amount of material is forming in front of the tool when the cutting

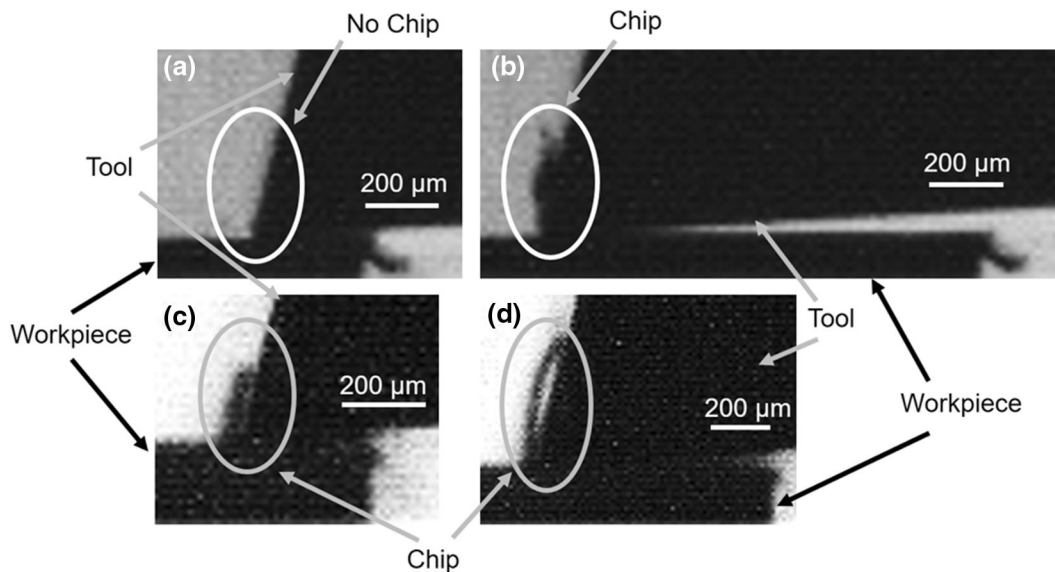


Fig. 6 Projection in the cutting plane of chips in formation for **a** $h = 1 \mu\text{m}$ after 0.6 ms of cut, **b** $h = 1 \mu\text{m}$ for a longer length of cut, **c** $h = 10 \mu\text{m}$ after 0.6 ms of cut, **d** $h = 10 \mu\text{m}$ for a longer length of cut

length increases; no chip is formed at the beginning of the cut. This phenomenon is also observed when the uncut chip thickness is $1 \mu\text{m}$. The amount of material is still smaller and the cutting length to form it larger. It will come off the workpiece when its size is larger enough, i.e. the minimum chip thickness is reached. Figure 7 shows that material accumulation in front of the edge radius when the cutting length increases, as well as the ejection of the material when the uncut chip thickness is large enough. Such a “chip” is therefore formed by a discontinuous mechanism. This is in accordance with the experiments. For these uncut chip thicknesses, the value of the rake angle has no influence anymore on the chip formation because the absence of contact on that zone. It only depends on the geometry of the cutting edge radius, leading to a configuration where the effective rake angle is negative; this was highlighted by Dornfeld et al. [3] in the literature review. The value of this negative effective rake angle increases when the uncut chip thickness decreases. In the modeling, the primary shear zone is widening and becomes hardly noticeable. It is moving under the tool radius. It can be observed in Fig. 7 that the area where the Von Mises stresses are high in the tool is larger when the material accumulation is significant (Fig. 7a, c). This area is smaller just after the ejection of the material (Fig. 7b, d) because the uncut chip thickness decreases to nearly $1 \mu\text{m}$ (smaller

than the minimum chip thickness), which leads to lower stresses.

Modeling results show that the minimum chip thickness is larger than the uncut chip thickness of $1 \mu\text{m}$ for which no chip is formed and the material is deformed then torn. When the tool moves, it deforms the workpiece and a fraction of the uncut chip thickness accumulates in front of the edge radius. This amount of material grows with the cutting length and it comes off the workpiece as soon as the minimum chip thickness is reached. This cutting mechanism is discontinuous and should end in variations in the cutting forces (this confirmed in the next paragraph). When the uncut chip thickness is $5 \mu\text{m}$, a chip is formed. Based on the cutting mechanism, the minimum chip thickness would be between 2.5 and $5 \mu\text{m}$. The numerical model produces chips close to the experimental ones. It is moreover able to model the cutting refusal, a feature only observed in the works of Lai et al. [44] for OFHC copper.

6.2 Cutting forces

Figure 8 shows the evolution of the numerical cutting and feed forces for the uncut chip thickness of $1 \mu\text{m}$. It is noted that the steady state for the cutting force is reached sooner ($\approx 20 \mu\text{s}$) than that of the feed

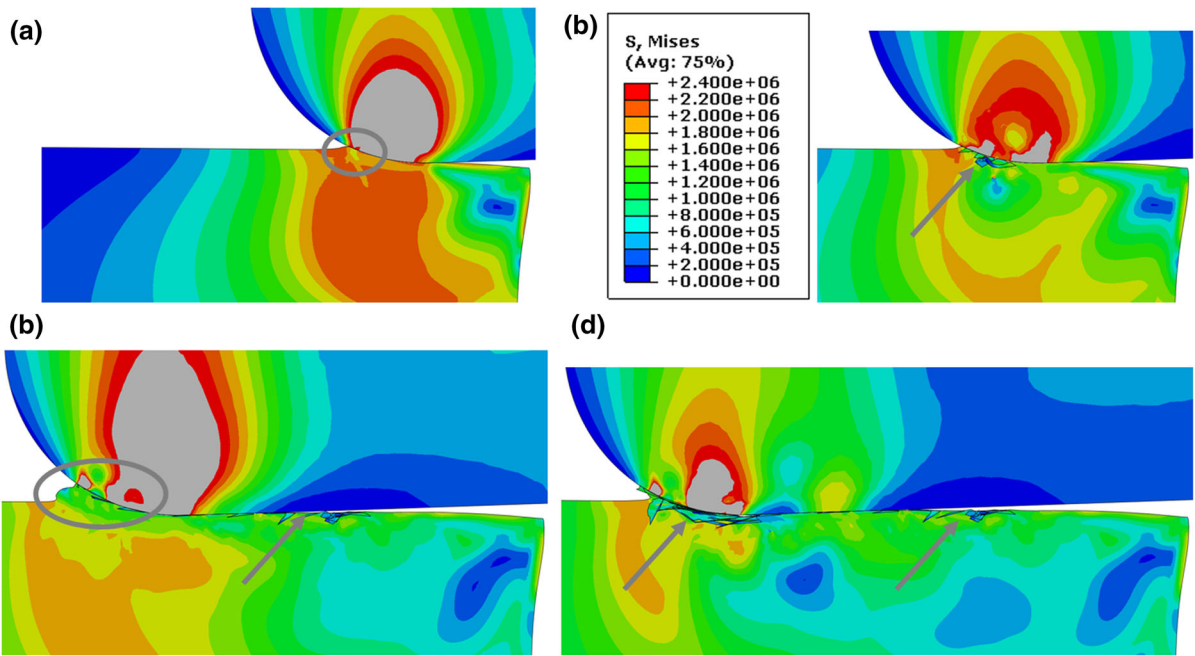


Fig. 7 Accumulation and ejection of material in front of the tool edge radius in the modeling for $h = 1 \mu\text{m}$ (arrows point ejected material, the accumulation of material is circled) after **a** 20 μs , **b** 25 μs , **c** 50 μs and **d** 60 μs of cut

force ($\approx 65 \mu\text{s}$). The feed force is moreover larger than the cutting force, contrary to what is classically observed for macro-cutting conditions. Although cutting lengths are rather short, they are assumed to be large enough to dissipate transient effects in the chip formation. Steady-state is obtained when the temporal evolutions of the cutting forces are constant (or periodical). It is assumed that thermal steady-state is reached at the same time or that thermal aspects do not influence significantly the results at the tool–chip interface. When the regime value is reached, the force remains constant except some drops. They correspond to the ejection of fractions of the amount of material formed in front of the tool, as expected. The material removals at small uncut chip thicknesses can therefore be identified by the drops in the forces they cause.

Filiz et al. [6] observed in micro-milling that the minimum chip thickness introduces variations in the cutting forces. They were due to absence of chip as long as the accumulation of material does not reach the minimum chip thickness value. The feed per tooth was too low and several teeth need to pass on the surface, leading to the bending of the micro-mill. This is consistent with the results of this study for the very small uncut chip thicknesses.

Root mean squares (RMS) values of the forces for each uncut chip thickness are summarized in Table 3. When $h = 1, \text{ and } 2.5 \mu\text{m}$, the steady state of chip formation is never reached due to the process described earlier. A stabilization of the cutting forces is however observed when the cutting length is large enough (Fig. 8). The RMS values presented in Table 3 are computed when that steady-state is reached. The numerical cutting force is globally close to the

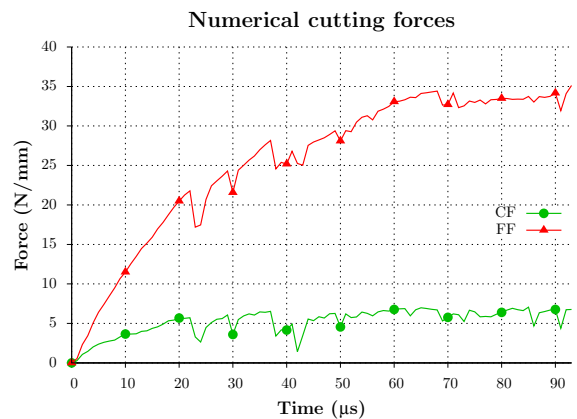


Fig. 8 Numerical cutting forces at $1 \mu\text{m}$

Table 3 Experimental (3 repetitions) and numerical RMS values of cutting and feed forces (CF and FF), Δ_{CF} : difference with the experimental values

h (μm)	CF_{Exp} (N/mm)	CF_{Num} (N/mm)	Δ_{CF} (%)	FF_{Exp} (N/mm)	FF_{Num} (N/mm)	Δ_{FF} (%)
280	387 ± 2	378	2	77 ± 4	106	-38
100	173 ± 2	179	-3	51 ± 1	105	-106
40	86 ± 2	68	21	41 ± 1	50	-22
20	51 ± 0.4	41	20	34 ± 0.4	44	-29
10	38 ± 0.8	26	32	32 ± 0.4	42	-31
5	22 ± 2	18	18	27 ± 1	36	4
2.5	21 ± 2	12	43	27 ± 2	35	-30
1	14 ± 2	6	57	24 ± 1	34	-42

experimental value, except at very small uncut chip thicknesses. The difference between the feed force values is quite large for the two largest uncut chip thicknesses, but it decreases for the others. For the two smallest, the difference for the cutting force is larger than for the feed force. The experimental cutting forces values are larger than the numerical ones, while it is the contrary for the feed forces. As expected, the forces are decreasing with the uncut chip thickness. Differences between modeled and experimental values are globally close to typical values observed in finite element modeling of machining [35, 45, 46]. They are larger for very small values of uncut chip thickness. As stated in the presentation of the experimental tests, a source of error can be found in the experiments: the positioning accuracy of the milling machine (1 μm) is no longer negligible in these cases. There is consequently an uncertainty on the corresponding cutting forces values. Flatness of the tenons may as well influence the actual uncut chip thickness.

Figure 9 presents the evolution of the ratio of the feed force on the cutting force for the eight values of the h/r ratio. Both curves have a nonlinear evolution. The simulated ratio is higher than the experimental one, which was expected as the cutting forces are close and the numerical feed forces larger. The inversion of the ratio occurs sooner for the modeling. As observed experimentally, the change in the cutting mechanism impacts the ratio between the feed and the cutting forces. Friction and deformations before the ejection of the material are much higher and can explain, at least partly, the growing importance of the feed force by comparison with the cutting force for small chip thicknesses (Fig. 9). The model captures this phenomenon accurately but it tends to overestimate the minimum chip thickness. A change in the cutting mechanism is observed when the uncut chip thickness is reduced: an inversion between

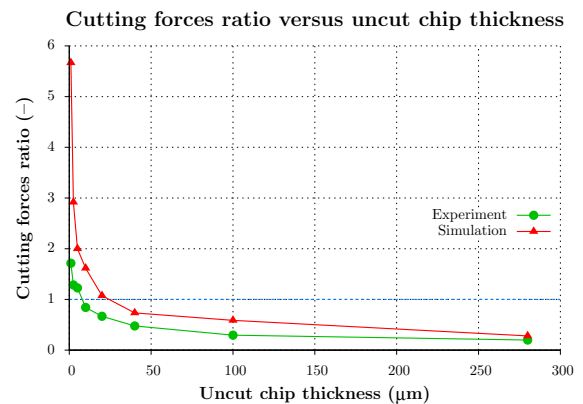


Fig. 9 Ratio of the cutting forces for the different h/r values

the cutting and feed forces occurs, as observed by Jun et al. [13]. The evaluation of the minimum chip thickness based on the inversion of the ratio of the forces leads to a value close to 5 μm .

6.3 Specific cutting energy

The specific cutting energy normalized by the value at 280 μm is presented, respectively, in Figs. 10 and 11 for the cutting force and the feed force. In all the cases, numerical or experimental, cutting or feed force, the size effect is observed as mentioned in the literature. Indeed, a nonlinear increase of the specific cutting energy is observed when the uncut chip thickness decreases. Curves are closer for the feed force at very small uncut chip thicknesses.

To give a point of comparison with specific cutting energies values that can be found in the literature for macro-cutting conditions, the specific cutting energies from Sun et al. [47] are provided in Table 4 together with experimental and numerical values of this study. No values in micro-cutting conditions are available in

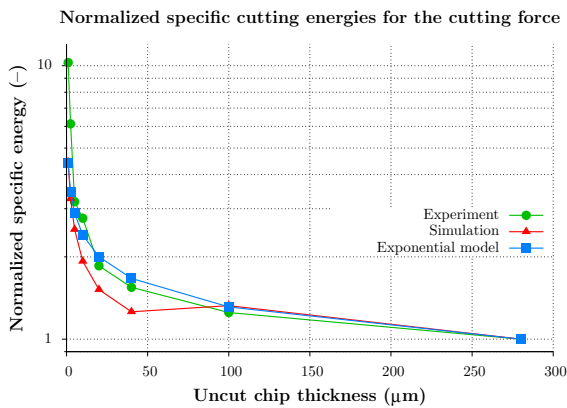


Fig. 10 Normalized specific cutting energy for the cutting force for the different h/r values

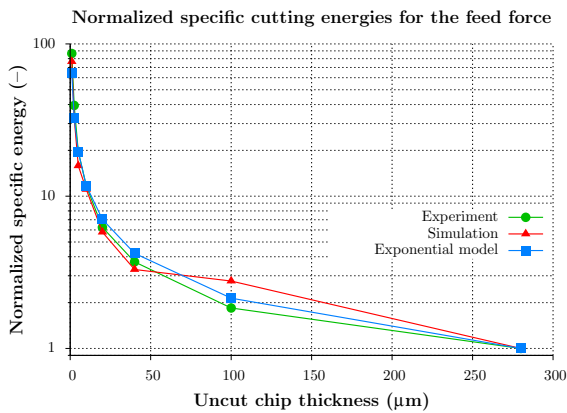


Fig. 11 Normalized specific cutting energy for the feed force for the different h/r values

the literature for the material machined in this paper, Ti6Al4V. The cutting speed of the experimental values of Sun et al. [47] is 75 m/min and longitudinal turning was performed. However, the uncut chip thickness is the same as the largest used in this study, 280 μm, and the rake angle is the same as well (15°). For both cutting force and feed force specific cutting energies, the comparison with the values in turning at

75 m/min shows that the differences are of the order of 15 %. The values obtained in macro-cutting are therefore similar to the results from the literature.

The specific cutting forces (K_c on cutting direction and K_f along feed direction) have been identified from the cutting forces of the numerical model. The size effect is taken into account and nonlinear regression is performed on the specific cutting energy on the cutting and feed directions. The experimental model proposed by Altintas [48] leads to a good correlation ($R^2 > 95 \%$). The specific cutting forces are then modeled as follow:

$$K_c \text{ [MPa]} = 857 h_{\text{[mm]}}^{-0.2632}, K_f \text{ [MPa]} = 143 h_{\text{[mm]}}^{-0.7397} \tag{2}$$

Both curves are plotted in Figs. 10 and 11, highlighting the exponential evolution of the specific cutting energy with the uncut chip thickness. The numerical model is again able to reproduce the experimental trends and the micro-cutting specificities identified in the literature.

The normalized specific cutting energy could be used to predict the uncut chip thickness. A threshold value of 2 for the normalized specific cutting energy for the cutting force is proposed. The experimental value would be this time larger than the numerical one.

6.4 Elastic spring-back of the workpiece

During the removal of material, an elastic spring-back of the workpiece is observed after the tool tip passage in the numerical model. This spring-back was only measured numerically. Figure 12 shows the evolution of the ratio (in %) between the elastic spring-back and the uncut chip thickness.

A nonlinear increase of the elastic spring-back is observed when the uncut chip thickness decreases. The ratio goes from around 0.2 % at 280 μm to 20 % for the uncut chip thickness of 1 μm. By comparison with the

Table 4 Experimental (from literature and this study) and numerical specific cutting forces (SCE) values for cutting and feed forces (CF and FF) at $h = 280\mu\text{m}$, Δ_x : difference with the experimental values from the literature reference

Case	SCE _{CF} (N/mm ²)	$\Delta_{\text{SCE}_{CF}}$ (%)	SCE _{FF} (N/mm ²)	$\Delta_{\text{SCE}_{FF}}$ (%)
Sun et al. [47]	≈ 1220	–	≈ 330	–
Exp.	1383	–13	274	17
Num.	1350	–11	379	–15

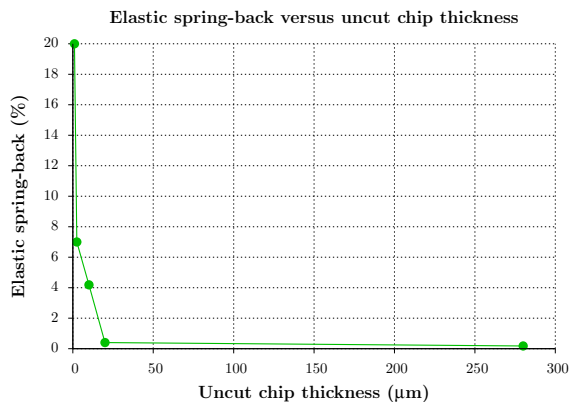


Fig. 12 Evolution of the elastic spring-back

uncut chip thickness, this ratio is thus growing when the uncut chip thickness is small, as mentioned in the literature. It contributes to the increase of the feed force, friction on the flank face and the specific cutting energy. The elastic spring-back of the workpiece can therefore not be neglected for the very small uncut chip thicknesses. It must be noted that the computed values should be considered as approximate values of the elastic spring-back due to the deletion of elements.

The elastic spring-back could be another indicator to evaluate the minimum chip thickness. The threshold value proposed is an elastic spring-back of 5 % of the uncut chip thickness. Based on Fig. 12, the minimum chip thickness is smaller than 10 μm: the evolution of the elastic spring-back becomes close to an exponential under this value.

7 Summary of the findings

An evolution of the chip morphology is observed, experimentally and numerically, when the uncut chip thickness decreases. The segments of the chip are less deep and the chip is no more regularly segmented. For very small uncut chip thicknesses, below 25 % of the tool edge radius, no chip is formed. The material accumulates then in front of the tool. When this amount of material reaches the minimum chip thickness, it comes off the workpiece; the material is more torn and deformed than sheared. The micro-cutting mechanism goes away from that of macro-cutting. The removal of material (i.e. chip formation), continuous in macro-cutting, becomes discontinuous.

Concerning the forces, some drops are observed on the nearly constant force evolution when the uncut chip thickness is small. They are due to the tearing of the material. This type of evolution shows clearly that the cutting process becomes discontinuous. The ratio of the feed force by the cutting force is smaller than one in macro-cutting. This ratio increases and becomes larger than one in micro-cutting. The inversion of that ratio means that the process is dominated by ploughing and friction. The model reproduces these features but tends to overestimate this ratio because the numerical feed force is larger than the experimental one. Values are however quite close and trends are well captured by the model, which is the aim of this study.

The decrease of the uncut chip thickness influences also the specific cutting energy. Indeed, it increases nonlinearly for small uncut chip thicknesses, highlighting the size effect characteristic of the micro-cut. Numerical normalized specific cutting energies were compared with that of the experiments and the evolutions were similar and close.

A nonlinear increase is also observed for the elastic spring-back of the workpiece in the numerical model. It takes more importance when the uncut chip thickness decreases and it cannot be neglected anymore for the very small uncut chip thicknesses for which it reaches 20 % of the material to remove.

From $h/r < 1$, the rake angle has no influence anymore on the chip formation: the material is in contact only with the cutting edge radius. The effective rake angle is negative and the tool cannot be considered as sharp. Only the value of the cutting edge radius of the tool influences the chip formation and ploughing becomes significant, as well as the elastic spring-back.

It is clear that the minimum chip thickness is not a single value but rather a range of values. According to the chip morphology and the cutting forces, the minimum chip thickness is between 2.5 and 5 μm. The value from the specific energy evolution would be less than 10 μm, which is confirmed by the numerical evolution of the elastic spring-back of the workpiece. In the end, the minimum chip thickness, for the cutting conditions and the material considered, would be higher than 2.5 μm, i.e. 25 % of the cutting edge radius of the tool. This value is close to what is generally observed in the literature for other materials and cutting conditions [6, 7, 9].

8 Conclusions

The experimental and numerical study of the influence of the uncut chip thickness on the chip formation showed that the morphology evolves and that the cutting refusal is reached when the uncut chip thickness is too low. An evolution in the chip formation process was identified and it became discontinuous for small uncut chip thicknesses, going away from that of macro-cutting. The modeled forces were globally close to the measurements as well as the evolution of the ratio of the feed force by the cutting force. The inversion of that ratio below very small values of the uncut chip thickness indicated the change in the mechanism. The specific cutting energy evolutions were nonlinear, in accordance with the size effect reported in the literature and experimentally observed. The numerical model gave information on the elastic spring-back of the workpiece. It increased significantly for the small uncut chip thicknesses and could not be neglected anymore.

The numerical model was able to produce results close to the experiments for the eight cutting conditions. The modifications in the chip formation mechanism due to the reduction of the uncut chip thickness were correctly handled. All the specificities of the micro-cutting were identified and close to the experimental values. The model allowed therefore to consider macro and micro orthogonal cutting with no other modification than the uncut chip thickness.

The minimum chip thickness has been estimated experimentally and numerically at minimum 25 % of the cutting edge radius and the results were in accordance. To go further, in orthogonal cutting, the heterogeneity of the machined material could be taken into account. The presented model is however able to give results close to the experiments and it reproduces qualitatively the trends, which may be enough depending on the required level of details.

Acknowledgments The authors gratefully acknowledge TechnoCampus for making their experimental resources available to us; Prof. P. Lambert from the *Université Libre de Bruxelles* for the high speed camera; and Dr F. Dagrain from the Department of Structural Mechanics of the UMONS Faculty of Engineering for giving us the opportunity to make some chip observations with the Keyence digital microscope.

References

- Chae J, Park SS, Freiheit T (2006) Investigation of micro-cutting operations. *Int J Mach Tools Manuf* 45:313–332
- Weule H, Hntrup V, Trischler H (2001) Micro-cutting of steel to meet new requirements in miniaturization. *Ann CIRP* 50:61–64
- Dornfeld D, Min S, Takeuchi Y (2006) Recent advances in mechanical micromachining. *Ann CIRP* 55:745–768
- Miao JC, Chen GL, Lai XM, Li HT, Li CF (2007) Review of dynamic issues in micro-end-milling. *Int J Adv Manuf Technol* 31:897–904
- Bissacco G, Hansen HN, De Chiffre L (2005) Micromilling of hardened tool steel for mould making applications. *J Mater Process Technol* 167:201–207
- Filiz S, Conley CM, Wasserman MB, Ozdoganlar OB (2007) An experimental investigation of micro-machinability of copper 101 using tungsten carbide micro-end-mills. *Int J Mach Tools Manuf* 47:1088–1100
- de Oliveira FB, Roger Rodrigues A, Teixeira Coelho R, Fagalide Souza A (2015) Size effect and minimum chip thickness in micromilling. *Int J Mach Tools Manuf* 89:39–54
- Bissacco G, Hansen HN, De Chiffre L (2006) Size effect on surface generation in micromilling of hardened tool steel. *Ann CIRP* 55:593–596
- Vogler MP, DeVor RE, Kapoor SG (2004) On the modeling and analysis of machining performance in micro end-milling, part I: surface generation. *J Manuf Sci Eng* 126:685–694
- Vogler MP, DeVor RE, Kapoor SG (2004) On the modeling and analysis of machining performance in micro end-milling, part II: cutting force prediction. *J Manuf Sci Eng* 126:695–705
- Vogler MP, DeVor RE, Kapoor SG (2003) Microstructure-level force prediction model for micromilling of multi-phase materials. *J Manuf Sci Eng* 125:202–209
- Ducobu F, Rivière-Lorphève E, Filippi E (2012) Dynamic simulation of the micro-milling process including minimum chip thickness and size effect. *Key Eng Mater* 504–506:1269–1274
- Jun MBG, DeVor RE, Kapoor SG (2006) Investigation of the dynamics of microend milling, part II: model validation and interpretation. *ASME* 128:901–912
- Liu X, DeVor RE, Kapoor SG (2006) An analytical model for the prediction of minimum chip thickness in micromachining. *ASME* 128:474–481
- Son SM, Lim HS, Ahn JH (2005) Effects of the friction coefficient on the minimum cutting thickness in micro cutting. *J Mach Tools Manuf* 45:529–535
- Son SM, Lim HS, Ahn JH (2006) The effect of vibration cutting on minimum chip thickness. *Int J Mach Tools Manuf* 46:2066–2072
- Liu X, DeVor RE, Kapoor SG, Ehman KF (2004) The mechanics of machining at the micro scale: assesment of the current state of the science. *J Manuf Sci Eng* 126:666–678
- Kim S-D, Kim DS (1995) Theoretical analysis of micro-cutting characteristics in ultra-precision machining. *J Mater Process Technol* 49:387–398

19. Liu K, Melkote SN (2007) Finite element analysis of the influence of tool edge radius on size effect in orthogonal micro-cutting process. *Int J Mech Sci* 49:650–660
20. Woon KS, Rahman M, Fang FZ, Neo KS, Liu K (2007) Investigations of tool edge radius effect in micromachining: a FEM simulation approach. *J Mater Process Technol* 167:316–337
21. Liu K, Melkote SN (2006) Material strengthening mechanisms and their contribution to size effect in micro-cutting. *Trans ASME* 128:730–738
22. Ohbuchi Y, Obikawa T (2003) Finite element modeling of chip formation in the domain of negative rake angle cutting. *ASME* 125:324–332
23. Simoneau A, Ng E, Elbestawi MA (2006) The effect of microstructure on chip formation and surface defects in microscale, mesoscale, and macroscale cutting of steel. *Ann CIRP* 55:97–102
24. Zhang YC, Mabrouki T, Nelias D, Gong YD (2011) Chip formation in orthogonal cutting considering interface limiting shear stress and damage evolution based on fracture energy approach. *Finite Elem Anal Des* 47:850–863
25. Ducobu F, Rivière-Lorphèvre E, Filippi E (2014) Numerical contribution to the comprehension of saw-toothed Ti6Al4V chip formation in orthogonal cutting. *Int J Mech Sci* 81:77–87
26. Ducobu F, Rivière-Lorphèvre E, Filippi E (2016) Material constitutive model and chip separation criterion influence on the modeling of Ti6Al4V machining with experimental validation in strictly orthogonal cutting condition. *Int J Mech Sci* 107:136–149
27. Mabrouki T, Girardin F, Asad M, Rigal J-F (2008) Numerical and experimental study of dry cutting for an aeronautic aluminium alloy (A2024–T351). *Int J Mach Tools Manuf* 48:1187–1197
28. Subbiah S, Melkote SN (2008) Effect of finite edge radius on ductile fracture ahead of the cutting tool edge in micro-cutting of Al2024-T3. *Mater Sci Eng A* 474:283–300
29. Chen G, Ren C, Yang X, Jin X, Guo T (2011) Finite element simulation of high-speed machining of titanium alloy (Ti–6Al–4V) based on ductile failure model. *Int J Adv Manuf Technol* 56:1027–1038
30. Zhang Y, Mabrouki T, Nelias D, Gong Y (2011) FE-model for titanium alloy (Ti–6Al–4V) cutting based on the identification of limiting shear stress at tool–chip interface. *Int J Mater Form* 4:11–23
31. Ducobu F, Arrazola P-J, Rivière-Lorphèvre E, Filippi E (2015) Comparison of several behaviour laws intended to produce a realistic Ti6Al4V chip by finite elements modelling. *Key Eng Mater* 651–653:1197–1203
32. Ducobu F, Rivière-Lorphèvre E, Filippi E (2015) On the introduction of adaptive mass scaling in a finite element model of Ti6Al4V orthogonal cutting. *Simul Model Pract Theory* 53:1–14
33. Calamaz M, Coupard D, Girod F (2008) A new material model for 2D numerical simulation of serrated chip formation when machining titanium alloy Ti–6Al–4V. *Int J Mach Tools Manuf* 48:275–288
34. Johnson GR, Cook WH (1983) A constitutive model and data for metals subjected to large strains, high strain rates and high temperatures. In: *Proceedings of the seventh international symposium on ballistics*, The Hague, The Netherlands, pp 541–547
35. Sima M, Özel T (2010) Modified material constitutive models for serrated chip formation simulations and experimental validation in machining of titanium alloy Ti–6Al–4V. *Int J Mach Tools Manuf* 50:943–960
36. Özel T, Zeren E (2007) Numerical modelling of meso-scale finish machining with finite edge radius tools. *Int J Mach Mach Mater* 2:451–768
37. Sun J, Guo YB (2009) Material flow stress and failure in multiscale machining titanium alloy Ti–6Al–4V. *Int J Adv Manuf Technol* 41:651–659
38. Lampman S (1990) Wrought titanium and titanium alloys, properties and selection: Nonferrous alloys and special-purpose materials. *ASM Handb ASM Int* 2:592–633
39. Nasr M, Ng E-G, Elbestawi M (2007) Effects of workpiece thermal properties on machining-induced residual stresses-thermal softening and conductivity. *Proc Inst Mech Eng B J Eng Manuf* 221:1387–1400
40. Ducobu F, Rivière-Lorphèvre E, Filippi E (2015) Experimental contribution to the study of the Ti6Al4V chip formation in orthogonal cutting on a milling machine. *Int J Mater Form* 8:455–468
41. Altintas Y (2012) *Manufacturing automation: metal cutting mechanics, machine tool vibrations, and CNC design*. Cambridge University Press, Cambridge
42. Mahnama M, Movahhedy MR (2010) Prediction of machining chatter based on FEM simulation of chip formation under dynamic conditions. *Int J Mach Tools Manuf* 50:611–620
43. SECO TOOLS (2011) *Turning catalog and technical guide 2012*. SECO TOOLS AB
44. Lai X, Li H, Li C, Lin Z, Ni J (2008) Modelling and analysis of micro scale milling considering size effect, micro cutter edgeradius and minimum chip thickness. *Int J Mach Tools Manuf* 48:1–14
45. Karpat Y (2011) Temperature dependent flow softening of titanium alloy Ti6Al4V: an investigation using finite element simulation of machining. *J Mater Process Technol* 211:737–749
46. Zhang YC, Mabrouki T, Nelias D, Gong YD (2011) Chip formation in orthogonal cutting considering interface limiting shear stress and damage evolution based on fracture energy approach. *Finite Elem Anal Des* 47:850–863
47. Sun S, Brandt M, Dargusch MS (2009) Characteristics of cutting forces and chip formation in machining of titanium alloys. *Int J Mach Tools Manuf* 49:561–568
48. Altintas Y (2000) *Manufacturing automation: metal cutting mechanics, machine tool vibrations and CNC design*. Cambridge University Press, Cambridge.